Fuzzy nanostructure growth on precious metals by He plasma irradiation

Shin Kajita

*Institute of Materials and Systems for Sustainability, Nagoya University, Nagoya 464-8603, Japan**

Tomohiro Nojima, Yudai Tomita, Noriyasu Ohno, Hirohiko Tanaka

Graduate School of Engineering, Nagoya University, 464-8603, Japan

Naoaki Yoshida

Research Institute for Applied Mechanics, Kyushu University, Kasuga, Fukuoka 816-8580, Japan

Miyuki Yajima, Tsuyoshi Akiyama, Masayuki Tokitani

National Institute for Fusion Science, Toki, Gifu 509-5292, Japan

Takashi Yagi

National Metrology Institute of Japan, National Institute of Advanced Industrial Science and Technology, Tsukuba, Ibaraki 305 8563, Japan

(Dated: February 5, 2018)

Abstract

Growth of helium bubbles near the surface of metals leads to various morphology changes when sufficient helium ions are continuously implanted on the surface. In this study, low energy (< 100 eV) helium plasma irradiations to various noble metals were conducted, and consequent surface morphology changes were analyzed. It was found that fiberform nanostructures were formed by the helium plasma irradiation on rhodium and ruthenium thin films, which were deposited by magnetron sputtering, and on platinum and iridium wires. Growth of fiberform structures were not identified on gold, silver, and palladium samples exposed to helium plasmas even though the irradiations were conducted at various surface temperatures, though pinholes were observed on palladium surface. We discussed the relation between the morphology changes and material properties.

PACS numbers:

*Electronic address: kajita.shin@nagoya-u.jp

I. INTRODUCTION

Implanted helium (He) atoms in metals have been known to be trapped, migrate inside the crystal structure, and form clusters and He bubbles [1]. Plasma irradiation experiments under fusion relevant conditions suggested that the implantation can occur even when the incident ion energy is much lower than ∼100 eV [2], which is not enough to form defects. Growth of He bubbles led to significant morphology changes on metal surfaces in nanoscale when certain irradiation conditions were satisfied [3–10]. The size and shape of the morphology changes were significantly altered by the material properties and the irradiation conditions, i.e., the melting point, the sputtering yield, the surface temperature, the incident ion energy, the helium flux / fluence and so on. One of the most significant changes found on various metals was the growth of fiberform fuzzy nanostructures [3]. It has been identified that the *fuzz* was grown on W when the surface temperature was in the range of 1000-2000 K and the incident ion energy was higher than ∼30 eV [11]; the temperature range was lower for molybdenum (Mo) (800 - 1050 K) than that on W [12]. In addition, nanocones were formed on titanium (Ti), iron (Fe), and stainless steel [5, 13], nano/micro-pillar structures were found on aluminum (Al) and cupper (Cu) [6], and cube shaped structures were identified on vanadium (V) [7] after helium plasma irradiation.

On the one hand, the changes in the material properties caused by the morphology change could be harmful for plasma facing component for thermonuclear fusion devices [14]; on the other hand, they could be used for industrial applications utilizing the advantages such as large effective surface area [15] and high optical absorptance [16]. One of the applications of fine structured metals formed by the He plasma irradiation is likely to be photocatalysis/catalysis. Metal oxides and/or (oxi)nitrides are regarded as the material for hydrogen production via solar water splitting [17, 18], which can be a solution of the energy problem in the 21st century. It was shown that nanostructured W partially oxidized exhibited significant visible light activity for methylene blue decomposition [5, 19] and five times enhanced photocurrent representing water splitting [20].

In this study, we investigated the effects of He plasma irradiation on noble metals. One of the reasons why we focused on noble metals is in the fact that they are regarded as highly active materials as catalysts/photocatalysts. In addition to popular titania supported platinum (Pt) catalysts [21], rhodium (Rh), Pt, and palladium (Pd) have been used to

control NO_x [22]. Moreover, gold nanoparticles have been used as various support materials [23], and ruthenium (Ru) and iridium (Ir) are also active catalysts such as for instance electro-catalytic reaction [24]. From He plasma irradiation experiments in a linear plasma device, it is shown that fuzzy nanostructures are grown easily on some metals, whereas those fine structures are hardly formed on other metals. Discussion will be provided in terms of the relation between the differences in the morphology changes and physical properties, in particular, shear strength, which is regarded as an important parameter for fuzz growth [25].

II. PREPARATION

Table I summarizes materials used for experiments in the present study: Ru, Rh, Pd, Ag, Ir, Pt, and Au. In addition to the atomic number and crystal structure, the melting point, T_m, the boiling point, and the shear modulus are presented. The atomic number are from 44 to 47 and from 77 to 79. All the materials except for Ru, which has hexagonal close packing crystal (HCP) structure, have face centered cubic (FCC) structure. The melting points of Ru, Rh, Ir, and Pt are higher than 2000 K, while those of Au and Ag are lower than 1500 K. It is worthwhile to note that some metals have significantly high shear modulus; the shear modulus of Ru, Rh and Ir at room temperature is 173, 150, and 210 GPa, which is comparable or higher than that of W (160 GPa).

He plasma irradiation was conducted in the linear plasma device NAGDIS-II (Nagoya Divertor Simulator). The detail of the experimental setup is described elsewhere [5]. The plasma is produced by a direct current (DC) arc discharge using a LaB_6 cathode heated with a carbon heater. Magnetic fields, the strength of which was $\sim$0.1 T, limited the radial plasma diffusion, and linear shaped plasma with the length of $\sim$2.5 m was produced in steady state. The background pressure gas was $\sim 10^{-4}$ Pa or less before the experiments. Additional He gas injection increased the pressure to $\sim$ 0.7 Pa during the He plasma irradiation. The He plasma irradiation was conducted at a downstream region $\sim$1.5 m far from the cathode. Typically the density was on the order of 10^{18} m^{-3}, and the temperature was $\sim$5 eV. The surface temperature, T_s, can be increased to higher than 1000 K without cooling. Thus, the sample was equipped on a water cooling stage with a Mo cover to control the surface temperature when the irradiation was conducted at the temperature of less than 1000 K. The surface temperature was measured by a radiation pyrometer. The incident ion energy,

E_i, was controlled by biasing the sample negatively. Note that the space potential of the plasma was about -5 eV, and E_i was determined from the biasing voltage and the space potential. The He flux was measured using an electrostatic probe, which was installed $\sim$ 0.3 m upstream from the sample.

Because some noble metals were expensive and difficult to be obtained as a bulk, we used thin film for Rh and Ru, thickness of which was typically $\sim$1 μm, formed by magnetron sputtering devices. Also, wires were used for Ir, Pt, Au, and Ag similar to Re case in [9]; the diameter of the wires is typically 0.2 mm. Wires were attached to a Mo or Ta plate by a spot wielding; we measured the plate temperature, and the temperature of the wire was assumed to be the same as that of the plate. Plates were used for irradiation experiments on Pd samples, because they were available.

III. IRRADIATION EXPERIMENTS

A. rhodium, ruthenium, iridium, and platinum

Let us start from metals which have high shear modulus and melting points, i.e., Rh, Ru, and Ir. Figure 1(a) shows a scanning electron microscope (SEM) micrograph of Rh surface exposed to the He plasma. The incident ion energy was 45 eV, T_s was 973 K, and the He fluence was 1.1 $\times 10^{26}$ m^{-2}. Fine nanostructures were grown with entangling together on the surface. The shape was slightly different from the fuzzy structures observed on W or Mo; many linearly extended Rh fibers were observed on the surface. For Rh or Ru, He plasma irradiation was conducted using $\sim$1 μm thick samples in this study. The influence of bulk layer was investigated using a W coated Mo samples, and it was shown that mixture of the material occurred around the boundary [26] In this study, it was confirmed from energy dispersive X-ray spectroscopy (EDS) analysis while conducting cross sectional observation that the surface structures were mainly composed of Rh or Ru under the present condition. No W signal was identified on Rh fiber and W/Ru ratio was less than 10% on Ru fibers. Figure 1(b) shows a transmission electron microscope (TEM) micrograph of the Rh fiberform structure. Many bubbles were identified in fibers; it was interesting to note that shape of some bubbles was not spherical or hexagonal shape observed on W bubbles [27] but elliptical. For some reason, it would be easier for bubbles to be expanded in the

radial direction compared with the axial direction.

Figure 2(a) shows an SEM micrograph of He irradiated Ru surface; E_i was ∼45 eV, T_s was 1193 K, and the He fluence was 3.3×10^{25} m^{-2}. After the He plasma irradiation, the surface was covered with linear shaped nanofibers. The linear shaped fibers were much denser than that in the cases of Rh sample. Figure 2(b) shows TEM micrographs of Ru fibers formed by the He plasma irradiation. Many bubbles were observed in nodes of fibers, but no bubbles were identified in the linearly elongated nanofibers. This indicated that the formation mechanisms of the linear fibers might have been different from fuzzy structures grown on other metals. Previously, formation of similar linear shaped fibers was identified on rhenium (Re) surface [9]. It is noted that both of Re and Ru have high shear modulus and HCP crystal structure.

Figures 3(a-c) show SEM micrographs of Ir surfaces exposed to the He plasmas at T_s of 980, 1273, and 1473 K, respectively; E_i was 85 eV for all the samples, and the He ion fluence was in the range of 1.8-7.5 $\times10^{25}$ m^{-2}. Fuzzy structure and membrane structure were observed partially at the edge of the sample at the surface temperature of 980 K. When T_s was increased to 1273 K or higher, fuzzy structures were identified on the surface. From the results so far, one can say that fuzzy nanostructures are easily grown on Rh, Ru, and Ir.

Figure 4(a,b) SEM micrographs of Pt surfaces exposed to He plasmas. The irradiation condition was as follows: T_s of 910 K, E_i of ∼80 eV, and the He fluence was 1.1×10^{26} m^{-2}. Note that the shear modulus of Pt is less than half of those of Ru, Rh, and Ir, as shown in Table I. Thin nanostructured layer were formed on the surface, similar to loop structures identified in the initial formation process of fuzzy structure [12]. However, different from Rh, Ru, and Ir, the fuzzy structures were not fully grown even though the fluence reached 10^{26} m^{-2}. Because the sputtering is almost negligible for Pt as was discussed previously [10], we can rule out the possibility that the thickness was determined from an equilibrium between the growth and erosion by sputtering [28]. Thus, the growth rate of nanostructures on Pt should be much lower than that on W.

B. palladium, silver, and gold

Figures 5(a-d) show SEM micrographs of Pd samples exposed to the He plasmas at the surface temperature of 490, 540, 700, and 950 K, respectively. The He fluences were in the

range of 2.0-9.0 $\times 10^{25}$ m^{-2}, and the incident ion energy was 45 eV. Various morphology changes were identified on the surface: cone shaped structures in Fig. 5(b), spheres in Fig. 5(c), and pinholes and wavy roughness in Fig. 5(d). Similar to Ti and iron, cones would have been formed with the help of sputtering [5], and pinholes were formed by the growth of He bubbles [29]. However, no fiberform structures were observed on the surface. On Pd, nanostructure growth was reported by the He plasma irradiation [30]; the irradiation was conducted using a He helicon plasma source in the surface temperature range of 650-800 K at an incident ion energy of $\sim$40 eV. Since the irradiation condition in this study seemed to be similar to the ones in [30], further investigation is required to find the potential reasons to cause the difference by conducting irradiation under different conditions, e.g., in the He flux and/or background pressure.

Figures 6(a,b) show SEM micrographs of Ag and Au, respectively; T_s, E_i, and the He fluence were 550 K, $\sim$45 eV, and 1.0×10^{26} m^{-2} in both of the cases. Cones were formed on Ag surface, probably due to sputtering similar to Pd surface. Surface became rough on Au sample in a scale less than 100 nm. However, no fiberform structures were found on Ag and Au samples as well.

One of the important processes determine the morphology change was physical sputtering especially for the cone formation on Pd and Ag seen in Figs. 5(b) and 6(a), respectively. It is known that cones were formed on metal surfaces by ion irradiation with the help of physical sputtering after protuberances were formed due to seed atoms [31]. In a similar manner, protuberances formed by He bubble growth can be the seeds for the growth of cone structures [5]. Concerning pinholes and wavy roughness in Fig. 5(d), they are included in typical morphology changes observed in the early stages of fuzz formation by He plasma irradiation (smooth, wavy , pyramidal or terraced/wide waves) [32]. It was revealed that the undulation height was approximately consistent with the depth of the heavily damaged layer due to helium plasma exposure and the interval of the undulating surface was related with the tilting angle from the 100 plane [33]. It is highly likely that the roughness observed on Pd surfaces was formed in the same mechanism as W cases. At the moment, the mechanism to form nano-spheres on Pd shown in Fig. 5(c) is not understood well.

IV. DISCUSSION

Table II summarizes the results of the irradiation experiments in this study. Fiberform nanostructures were easily formed on Ru, Rh, and Ir; they were grown on Pt as well when increasing the He fluence, but no fiberform structure growth was identified on Pd, Ag, and Au. On Pd, Ag, and Au, fine fiberform structures were not grown even though we conducted irradiation as changing the surface temperature. At the moment we cannot deny the possibility of the fiberform nanostructure growth on Pd, Ag and Au; fine structure may be grown on Pd, Ag, and Au when we control the irradiation condition further, e.g., decreasing T_s or increasing the fluence or E_i. However, we can at least say that there is a difficulty to form fine structures on those metal surfaces.

Following the viscoelastic model describing the growth of fiberform structure, material flow in the skin of fibers is thought to be the key process of the growth [34]. The model have explained the several key features of the fuzz growth, i.e., $t^{1/2}$ dependence of the fiber length the and the temperature dependence of the growth rate. In the model, shear stresses created due to the formation of new bubbles at the fiber tip is an important factor. Although the high ideal shear strength of pure W may not facilitate the plastic mechanism of fuzz formation, molecular dynamics modeling showed that the shear stress decreases by increasing the temperature and He concentration in metal [25]. In other words, the shear modulus can be an important factor as having a shear modulus window for fuzz growth [9]. From that point of view, the shear modulus and sputtering yield were summarized in [10], and the relation with nanostructure growth feature was discussed.

Here, in Fig. 7, we summarize the fiberform nanostructure growth features using different markers in terms of the shear modulus and T_m for the noble metals used in the present study (red markers) and reported metals (black markers). Here, the shear modulus in the temperature range of $0.25T_m$ to $0.5T_m$ was plotted using error bars by considering the temperature dependences for Rh and Ir [35], Ru [36], Au [37], Ag [38], and other metals (references in [10]). The temperature range of 0.25-$0.5T_m$ roughly corresponds to the empirically obtained necessary temperature range for the growth of W fuzz. The growth of He bubbles are thought to be important processes for the nanostructure growth by He plasma irradiation, and the migrations of He atoms/clusters, which control the growth of He bubbles in metals, are altered significantly by the material temperature. When the sur-

face temperature is higher than the temperature range, the size of the bubbles becomes too large and microstructures are formed. On the other hand, no significant morphology changes occur when the surface temperature is lower than the temperature range, because significant He diffusion and bubble growth are not activated [13]. As described, the shear modulus would decrease with increasing the concentration of He atoms in W as well. It could be less than half if the atomic concentration of He was 10% [25]. Although the effect of He concentration on the shear modulus is not included in Fig. 7, the bulk shear modulus without He concentration can be an index to see the tendency of the nanostructure growth.

Morphology changes can be categorized three different types in terms of fiberform nanostructure growth : (i) fiberform nanostructure is easily formed, (ii) only thin layer formation, and (iii) no fiberform nanostructure formation. We excluded titanium from those categories, because nanostructure growth was only once identified locally on the surface when the He fluence is high [13]; it would be positioned in between (ii) and (iii). Concerning Ir, Ru, and Rh, they are categorized in (i), in addition to the previously reported W, Re, and Mo. All of those metals have high melting point (> 2000 K) and high shear modulus (>100 GPa). Pt would be categorized in (ii), in addition to previous reported Ta, Fe, and Ni. Although the range of the melting point is wide from 1700 to 3300 K, the shear modulus of those metals are in the range between 50-80 GPa. The metals on which no fiberform nanostructure growth was identified have all low melting point (<2000 K) and low shear modulus (<50 GPa). Thus, for Au, Ag, and Pd, the shear modulus might have been too low to form nanostructures by He plasma irradiation.

As was discussed, the surface temperature is an important factor for the fiberform nanostructure growth, and normalized temperature to the melting point is an index to explain the bubble growth [39]. Figure 8 summarize the temperature ranges where fiberform nanostructures were grown on various metals. All the materials on which fiberform nanostructure growth occurred in Fig. 7, i.e., W, Re, Ta, Mo, Ir, Ru, Rh, Pt, Ti, Fe, and Ni, are plotted. The temperature ranges for the fiberform nanostructure growth have been clearly revealed on W and Mo. The nanostructure W growth occurred in the range of 1000-2000 K, which corresponded to T_s/T_m of 0.27-0.54, and Mo nanostructure growth occurred in the range of 800-1050 K [12], which corresponded to T_s/T_m of 0.28-0.36; those were presented in Fig. 8 with orange bars. Dotted lines in Fig. 8 correspond to T_s/T_m =0.6 and 0.25; all the conditions for the other metals were plotted in between the two dotted lines. The temperature

window of W in terms of T_s/T_m was wider than that of Mo. Although sufficient experiments have yet to be done on Ir, the temperature window of Ir would be wider than Mo. The fuzz growth occurred on Ir even at T_s/T_m of 0.54, whereas the maximum T_s/T_m for the fuzz growth on Mo was 0.36. This may be reasonable considering the facts that the shear modulus decreases with increasing the temperature and Ir and W have higher shear modulus than that of Mo. In other words, the fine structure growth might not occur for the high region in T_s/T_m, namely > 0.36 for Mo, when the shear modulus of the material was lower than Ir and W. We conducted He plasma irradiation at T_s/T_m of 0.45 for Ag and 0.45 for Au. Because the shear modulus of Au and Ag was much lower than W, temperature might have been too high in terms of T_s/T_m. If we could conduct irradiation around the room temperature, fine structure growth might occur on those metals as well, though it requires a special cooling system. Of course, this is not always true; T_s/T_m range of fuzz growth for Fe was high (0.5-0.6), though the shear modulus was lower than Mo. Thus, it would be necessary to consider other factors to explain all; target temperature range can be roughly determined in terms of T_s/T_m when we conduct irradiation experiments to other metals in future.

V. CONCLUSIONS

Helium plasma irradiations were conducted using the linear plasma device NAGDIS-II on various precious metals: rhodium (Rh), ruthenium (Ru), iridium (Ir), platinum (Pt), gold (Au), silver (Ag), and palladium (Pd). Surface morphology changes were analyzed by scanning electron microscope and transmission electron microscope. Fine nanostructures were easily formed on Rh, Ru and Ir, which have high shear modulus (>150 GPa). He bubbles were observed inside fine structures on Rh and Ru. However, shape of the bubbles in Rh was not spherical, but it had elliptical shape elongated radially in the fiber. Moreover, on Ru fibers, no bubbles were observed on the linear shaped fibers, though many bubbles existed at the node of fibers. It was suggested that linear shaped Ru fiber might have grown in different growth process. On Pt, loop structures were identified on the surface. However, no fuzz has been identified Au, Ag, and Pd, which has low shear modulus (< 50 GPa).

The growth conditions were discussed in terms of the shear modulus and the surface temperature normalized to the melting point, T_s/T_m. Summarizing the results of irradia-

tion experiments that have been reported and investigated in this study, one can say that fiberform nanostructure could be easily grown on high shear modulus metals (>100 GPa), thin nanostructured layer could be formed on for the metal whose shear modulus was in the range of 50-100 GPa, and that fine structures were difficult to be formed on low shear modulus metals (< 50 GPa). The experimental results supported that shear modulus is an important physical values to form fine nanostructures by He plasma irradiations. The temperature range of the fiberform nanostructure growth was in the range of $0.25 < T_s/T_m < 0.6$ for all the metals on which fiberform nanostructure growth was identified.

This study showed that fiberform nanostructure growth can occur on various noble metals. For application, combination of thin film deposition and He irradiation using plasmas could be effective processes for these precious metals. It is of interests to investigate catalytic/photocatalytic properties using those nanostructures in future.

Acknowledgment

This work was supported in part by a Grant-in-Aid for Scientific Research (B) 15H04229 and a Grant-in-Aid for Exploratory Research 16K13917 from the Japan Society for the Promotion of Science (JSPS).

[1] W. Wilson, C. Bisson, M. Baskes, Self-trapping of helium in metals, Physical Review B, 24 (1981) 5616.

[2] D. Nishijima, M. Y. Ye, N. Ohno, S. Takamura, Incident ion energy dependence of bubble formation on tungsten surface with low energy and high flux helium plasma irradiation, J. Nucl. Mater., 313-316 (2003) 97–101.

[3] S. Takamura, N. Ohno, D. Nishijima, , S. Kajita, Formation of nanostructured tungsten with arborescent shape due to helium plasma irradiation, Plasma Fusion Res., 1 (2006) 051.

[4] M. Baldwin, R. Doerner, Helium induced nanoscopic morphology on tungsten under fusion relevant plasma conditions, Nucl. Fusion, 48 (2008) 035001 (5pp).

[5] S. Kajita, T. Yoshida, D. Kitaoka, R. Etoh, M. Yajima, N. Ohno, H. Yoshida, N. Yoshida, Y. Terao, Helium plasma implantation on metals: Nanostructure formation and visible-light photocatalytic response, J. Appl. Phys., 113 (2013) 134301.

[6] I. Tanyeli, L. Marot, D. Mathys, M. C. M. van de Sanden, G. D. Temmerman, Surface modifications induced by high fluxes of low energy helium ions, Sci. Rep., 5 (2015) 9779.

[7] J. Tripathi, T. Novakowski, A. Hassanein, Tuning surface porosity on vanadium surface by low energy he+ ion irradiation, Appl. Surf. Sci., 378 (2016) 63 – 72.

[8] K. Omori, A. M. Ito, K. Shiga, N. Yamashita, K. Ibano, H. T. Lee, Y. Ueda, Comparison between helium plasma induced surface structures in group 5 (Nb, Ta) and group 6 elements (Mo, W), Journal of Applied Physics, 121 (2017) 155301.

[9] S. Takamura, Y. Uesugi, Experimental identification for physical mechanism of fiber-form nanostructure growth on metal surfaces with helium plasma irradiation, Appl. Surf. Sci., 356 (2015) 888 – 897.

[10] S. Kajita, T. Ishida, N. Ohno, D. Hwangbo, T. Yoshida, Fuzzy nanostructure growth on Ta/Fe by He plasma irradiation, Sci. Rep., 6 (2016) 30380.

[11] S. Kajita, W. Sakaguchi, N. Ohno, N. Yoshida, T. Saeki, Formation process of tungsten nanostructure by the exposure to helium plasma under fusion relevant plasma conditions, Nucl. Fusion, 49 (2009) 095005.

[12] S. Takamura, Temperature range for fiber-form nanostructure growth on molybdenum surfaces due to helium plasma irradiation, Plasma Fusion Res., 9 (2014) 1405131.

[13] S. Kajita, D. Kitaoka, N. Ohno, R. Yoshihara, N. Yoshida, T. Yoshida, Surface modification of titanium using he plasma, Appl. Surf. Sci., 303 (2014) 438 – 445.

[14] S. Kajita, G. D. Temmerman, T. Morgan, S. van Eden, T. de Kruif, N. Ohno, Thermal response of nanostructured tungsten, Nucl. Fusion, 54 (2014) 033005.

[15] M. Yajima, Y. Hatano, S. Kajita, J. Shi, M. Hara, N. Ohno, Tritium retention in nanostructured tungsten with large effective surface area, J. Nucl. Mater., 438 (2013) S1142–S1145.

[16] S. Kajita, T. Saeki, N. Yoshida, N. Ohno, A. Iwamae, Nanostructured black metal: Novel fabrication method by use of self-growing helium bubbles, Appl. Phys. Exp., 3 (2010) 085204.

[17] A. Fujishima, K. Honda, Electrochemical photolysis of water at a semiconductor electrode, Nature, 238 (1972) 5358.

[18] A. Kudo, Y. Miseki, Heterogeneous photocatalyst materials for water splitting, Chemical Society Reviews, 38 (2009) 253–278.

[19] K. Komori, T. Yoshida, T. Nomoto, M. Yamamoto, C. Tsukada, S. Yagi, M. Yajima, S. Kajita, N. Ohno, Sulfur k-edge XANES for methylene blue in photocatalytic reaction over WO3 nanomaterials, Nucl. Instruments and Methods in Phys. Res. Section B, 365, Part A (2015) 35 – 38.

[20] M. de Respinis, G. De Temmerman, I. Tanyeli, M. C. van de Sanden, R. P. Doerner, M. J. Baldwin, R. van de Krol, Efficient plasma route to nanostructure materials: Case study on the use of m-WO3 for solar water splitting, ACS Appl. Mater. & Interfaces, 5 (2013) 7621–7625.

[21] H. G. Manyar, C. Paun, R. Pilus, D. W. Rooney, J. M. Thompson, C. Hardacre, Highly selective and efficient hydrogenation of carboxylic acids to alcohols using titania supported pt catalysts, Chemical Communications, 46 (2010) 6279–6281.

[22] J. N. Armor, Environmental catalysis, Appl. Catalysis B: Environmental, 1 (1992) 221 – 256.

[23] M. Haruta, Gold as a novel catalyst in the 21st century: Preparation, working mechanism and applications, Gold Bulletin, 37 (2004) 27–36.

[24] T. Reier, M. Oezaslan, P. Strasser, Electrocatalytic oxygen evolution reaction (OER) on Ru, Ir, and Pt catalysts: A comparative study of nanoparticles and bulk materials, ACS Catalysis, 2 (2012) 1765–1772.

[25] R. Smirnov, S. Krasheninnikov, On the shear strength of tungsten nano-structures with embedded helium, Nucl. Fusion, 53 (2013) 082002.

[26] P. Fiflis, N. Connolly, D. Ruzic, Experimental mechanistic investigation of the nanostructuring

of tungsten with low energy helium plasmas, J. Nucl. Mater., 482 (2016) 201 – 209.

[27] S. Kajita, N. Yoshida, R. Yoshihara, N. Ohno, M. Yamagiwa, TEM observation of the growth process of helium nanobubbles on tungsten: Nanostructure formation mechanism, J. Nucl. Mater., 418 (2011) 152 – 158.

[28] R. Doerner, M. Baldwin, P. Stangeby, An equilibrium model for tungsten fuzz in an eroding plasma environment, Nucl. Fusion, 51 (2011) 043001.

[29] S. Kajita, N. Yoshida, N. Ohno, Y. Tsuji, Growth of multifractal tungsten nanostructure by he bubble induced directional swelling, New Journal of Phys., 17 (2015) 043038.

[30] P. Fiflis, M. Christenson, N. Connolly, D. Ruzic, Nanostructuring of palladium with low-temperature helium plasma, Nanomaterials, 5 (2015) 2007–2018.

[31] G. K. Wehner, Cone formation as a result of whisker growth on ion bombarded metal surfaces, J. Vacuum Sci. Technol. A: Vacuum, Surfaces, and Films, 3 (1985) 1821 –1835.

[32] C. Parish, H. Hijazi, H. Meyer, F. Meyer, Effect of tungsten crystallographic orientation on he-ion-induced surface morphology changes, Acta Materialia, 62 (2014) 173 – 181.

[33] R. Sakamoto, E. Bernard, A. Kreter, C. Martin, B. Pegourie, G. Pieters, B. Rousseau, C. Grisolia, N. Yoshida, Surface morphology in tungsten and rafm steel exposed to helium plasma in psi-2, Physica Scripta, 2017 (2017) 014062.

[34] S. I. Krasheninnikov, Viscoelastic model of tungsten 'fuzz' growth, Physica Scripta, 2011 (2011) 014040.

[35] J. Merker, D. Lupton, M. Töpfer, H. Knake, High temperature mechanical properties of the platinum group metals, Platinum Metals Review, 45 (2001) 74–82.

[36] E. P. Papadakis, K. A. Fowler, L. C. Lynnworth, A. Robertson, E. D. Zysk, Ultrasonic measurements of young's modulus and extensional wave attenuation in refractory metal wires at elevated temperatures with application to ultrasonic thermometry, J. Appl. Phys., 45 (1974) 2409–2420.

[37] S. Collard, R. McLellan, High-temperature elastic constants of gold single-crystals, Acta Metallurgica et Materialia, 39 (1991) 3143 – 3151.

[38] J. P. Andrews, The variation of young's modulus at high temperatures, Proceedings of the Physical Society of London, 37 (1924) 169.

[39] J. H. Evans, Breakaway bubble growth during the annealing of helium bubbles in metals, J. Nucl. Mater., 334 (2004) 40–46.

TABLE I: Materials used for experiments: Ru, Rh, Pd, Ag, Ir, Pt, and Au. Atomic number, crystal structure, melting point, boiling point, and shear modulus at room temperature are shown.

	Ruthenium (Ru)	Rhodium (Rh)	Palladium (Pd)	Silver (Ag)	Iridium (Ir)	Platinum (Pt)	Gold (Au)
Atomic number	44	45	46	47	77	78	79
Crystal structure	HCP	FCC	FCC	FCC	FCC	FCC	FCC
Melting point [K]	2607	2237	1828	1235	2739	2041	1337
Boiling point [K]	4423	3970	3236	2435	4403	4098	2973
Shear modulus [Gpa]	173	150	44	30	210	61	27

TABLE II: Summary of the condition and results of the irradiation experiments in this study.

Material	E_i [eV]	He fluence $\times 10^{25}$ [m^{-2}]	T [K]	T_s/T_m	Morphology change
Rh	45	11	973	0.43	fiberform nanostructure
Ru	45	3.3	1193	0.46	fiberform nanostructure
Ir	85	7.5	980	0.39	membrane & fiberform nanostructure (locally)
Ir	85	2.6	1273	0.46	fiberform nanostructure
Ir	85	1.8	1473	0.54	fiberform nanostructure
Pt	80	11	910	0.45	loop
Pd	45	7.3	490	0.27	no change
Pd	45	2.0	540	0.30	cones
Pd	45	6.5	700	0.38	sphere
Pd	45	9.0	950	0.51	rough
Ag	45	10	550	0.45	cones
Au	45	10	550	0.41	rough

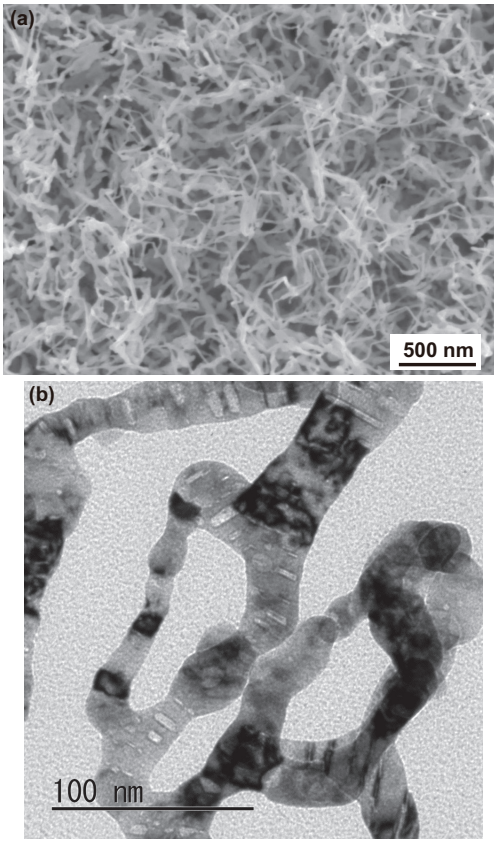

FIG. 1: (a) SEM and (b) TEM micrographs of Rh surface exposed to the He plasma. The irradiation condition was as follows: the incident ion energy of 45 eV, the surface temperature of 973 K, and the He fluence of 1.1 $\times 10^{26}$ m^{-2}.

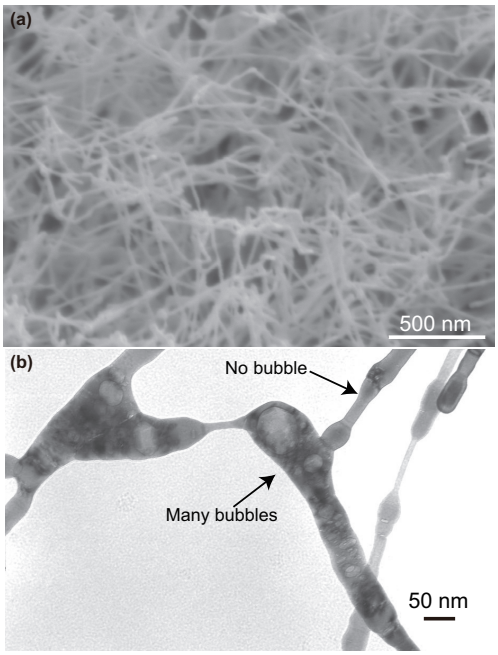

FIG. 2: (a) SEM and (b) TEM micrographs of He irradiated Ru surface. The incident ion energy was ∼45 eV, the surface temperature was 1193 K, and the He fluence was 3.3×10^{25} m^{-2}.

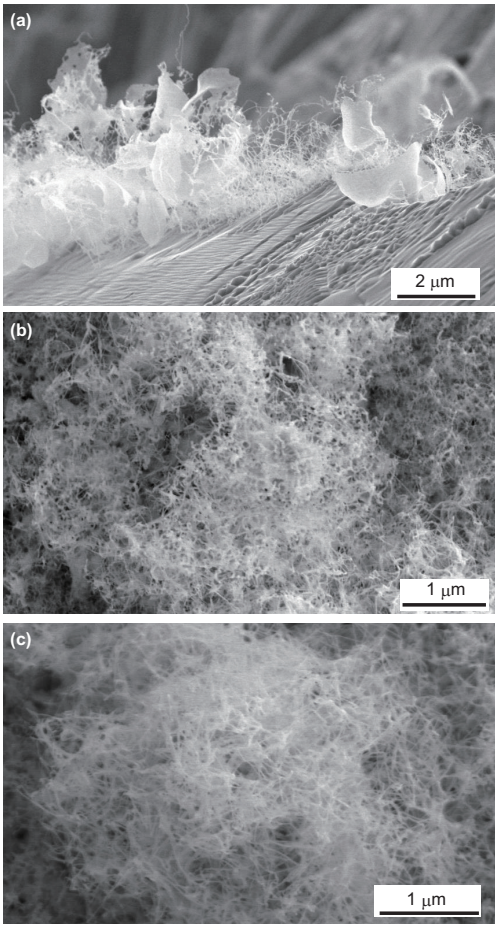

FIG. 3: SEM micrographs of Ir surfaces exposed to the He plasmas at the surface temperature of (a) 980, (b) 1273, and (c) 1473 K. The incident ion energy was 85 eV for all the samples, and the He ion fluence was in the range of 7.5, 2.6, and 1.8 $\times 10^{25}$ m^{-2}.

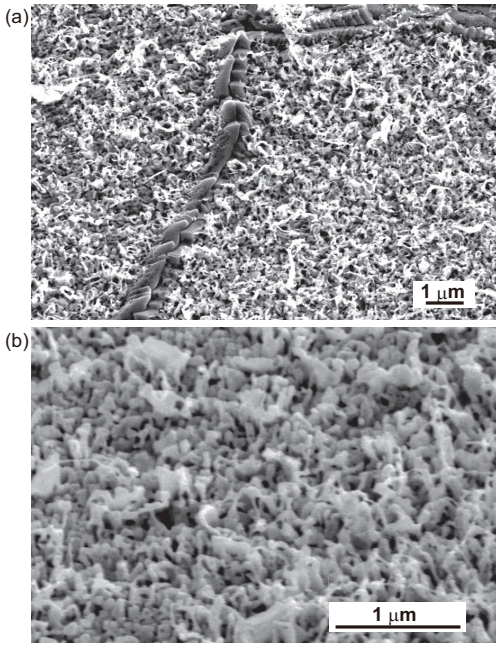

FIG. 4: SEM micrographs of Pt surfaces exposed to He plasmas. The irradiation condition was as follows: the surface temperature of 910 K, the incident ion energy of 80 eV, and the He fluence of the order of 10^{26} m^{-2}.

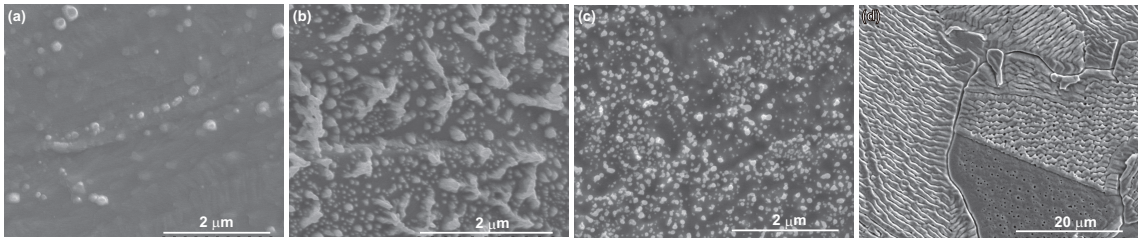

FIG. 5: SEM micrographs of Pd samples exposed at different temperatures (a) 490, (b) 540, (c) 700, and (d) 950 K. The He fluences were (a) 7.3 $\times 10^{25}$, (b) 2.0 $\times 10^{25}$, (c) 6.5 $\times 10^{25}$, and (d) 9.0 $\times 10^{25}$ m^{-2}.

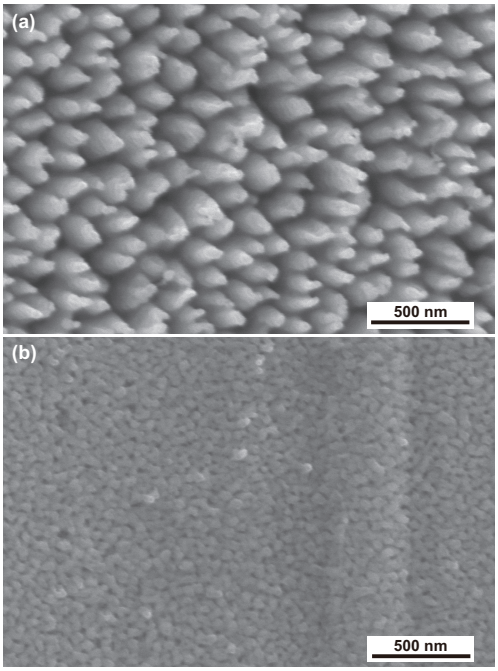

FIG. 6: SEM micrographs of (a) Ag, and (b) Au exposed to He plasmas. In both cases, E_i was 45 eV, T_s was 550 K, and the ion fluence was 1.0×10^{26} m^{-2}.

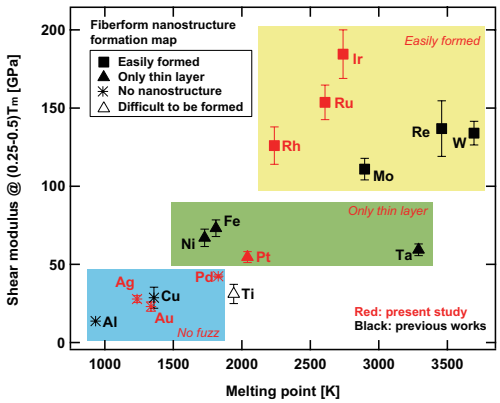

FIG. 7: The fiberform nanostructure growth feature were presented using different markers and plotted in terms of the melting point, T_m, and the shear modulus. The shear modulus was averaged value between $0.25T_m$ and $0.5\ T_m$, and the error bars represent the minimum and maximum values in the temperature region.

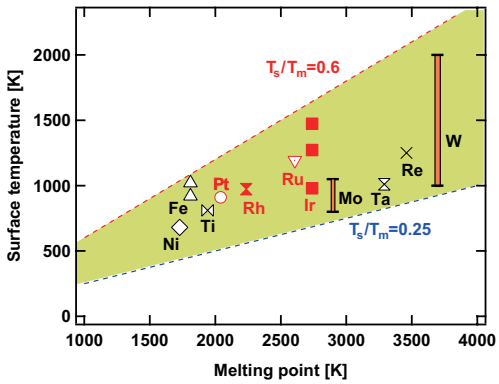

FIG. 8: Surface temperatures where fiberform nanostructure growth occurred shown as a function of the melting point on various metals. Black colored markers are the cases that have been reported and red colored markers represents the cases investigated in this study.